

Top-down fabrication of large-area GaN micro- and nanopillars

Ratan Debnath^{a)}

Material Science and Engineering Division, National Institute of Standards and Technology, Gaithersburg, Maryland 20899 and N5 Sensors Inc., Rockville, Maryland 20852

Jong-Yoon Ha^{a)}

Material Science and Engineering Division, National Institute of Standards and Technology, Gaithersburg, Maryland 20899 and Institute for Research in Electronics and Applied Physics, University of Maryland, College Park, Maryland 20742

Baomei Wen

Material Science and Engineering Division, National Institute of Standards and Technology, Gaithersburg, Maryland 20899 and N5 Sensors Inc., Rockville, Maryland 20852

Dipak Paramanik

Material Science and Engineering Division, National Institute of Standards and Technology, Gaithersburg, Maryland 20899

Abhishek Motayed^{b)}

Material Science and Engineering Division, National Institute of Standards and Technology, Gaithersburg, Maryland 20899 and Institute for Research in Electronics and Applied Physics, University of Maryland, College Park, Maryland 20742

Matthew R. King

Northrop Grumman ES, Linthicum, Maryland 21090

Albert V. Davydov

Material Science and Engineering Division, National Institute of Standards and Technology, Gaithersburg, Maryland 20899

(Received 28 October 2013; accepted 3 February 2014; published 19 February 2014)

Large-area gallium nitride (GaN) micro- and nanopillar (NP) arrays were fabricated by plasma etching of lithographically patterned GaN thin-film grown on Si substrate. Deep-ultraviolet lithography, inductively coupled plasma (ICP) etching, and subsequent chemical treatments were effectively utilized to fabricate GaN pillars with diameters ranging from 250 nm to 10 μm . The impact of various plasma etching process parameters and chemical etchants on the morphology, strain, and surface defects of these NPs were studied using scanning-electron microscopy, photoluminescence (PL), and Raman spectroscopy. It was found that the shape of the NPs can be controlled by the substrate temperature during the plasma etch and by using different gas chemistries. Room-temperature PL and Raman spectroscopy measurements revealed significant strain relaxation in 250 nm diameter pillars as compared to 10 μm diameter pillars. PL measurement also indicated that the surface damage from the plasma etch can be removed by etching in KOH-ethylene glycol solution. Post-ICP selective wet chemical etch enabled us to fabricate functional structures such as micro- and nanodisks of GaN, which potentially could be utilized in nitride-based resonators and lasers. © 2014 American Vacuum Society. [<http://dx.doi.org/10.1116/1.4865908>]

I. INTRODUCTION

Due to significant advances in epitaxial growth technology and fabrication techniques, gallium nitride (GaN) and related ternary alloys are presently gaining tremendous technological significance.^{1–4} However, there are still significant challenges to be solved including control of strain, defect reduction, and mitigation of unwanted polarization fields. Nanostructures provide some intriguing possibilities for resolving those challenges and improving device performance. Most research on nitride nanostructures has focused on bottom-up growth methods.^{5–9} Despite superior material quality and device performance in those fabricated structures, lack of large-area control of dimensions, morphology,

and orientation are problematic for device applications. Top-down fabrication methods provide an alternative route for producing of GaN micro- and nanopillar (NP) arrays from epitaxially grown thin films. Using similar top-down fabrication methods, nanostructures have also been realized in other material systems.^{10–12} Combination of lithography and etching techniques enables scalable fabrication of such pillars with excellent dimensional control, uniformity, and optical quality.^{13–15} The NP arrays can act as strain-free templates for subsequent epitaxial growth of n- and p-type group III-nitride structures enabling electrically active junctions along the semi- and nonpolar planes.

In order to produce NP arrays for device applications, top-down fabrication methods should have following attributes: (1) precise control over dimensions, shape, and morphology, (2) etch-damage free surfaces, (3) tailored profiles for specific applications, and (4) large-area uniformity and scalability.

^{a)}Debnath and Ha contributed equally to the work.

^{b)}Author to whom correspondence should be addressed; electronic addresses: amotayed@umd.edu; amotayed@nist.gov

Development of NP arrays with high aspect ratios (10 and higher) and diameters in the range of 150–250 nm require careful design of the etch process and selection of the mask material. It is also essential to analyze and control the surface defects as well as strain in the fabricated NP arrays. Obtaining smooth and defect-free sidewalls is also crucial for the subsequent selective epitaxial overgrowth.

In this article, we report the fabrication of GaN micro- and nanopillars with variety of shapes and sizes using different plasma etch chemistries and process conditions. Room-temperature photoluminescence (PL) and Raman spectroscopy measurements revealed different levels of strain relaxation depending on the NP shape and size. Wet chemical etching in KOH is shown to further improve the optical and surface quality of the fabricated pillars by removing the plasma-damaged material from the side-walls. Additionally, formation of GaN micro- and nanodisks using selective Si etch is also shown, which could potentially be used for developing resonators and emitters.

II. EXPERIMENT

Nominally undoped 0.8–1.5 μm thick GaN epitaxial layers grown by metalorganic chemical vapor deposition on a 4-in. Si (111) substrate were used in this study. Intermediate $\text{Al}_{1-x}\text{Ga}_x\text{N}$ buffer layers with varying x and thickness of 150 nm were grown on Si (111) prior to GaN growth. After the GaN growth, 50 nm of Si_3N_4 was deposited on the entire wafer. The GaN wafers were patterned using deep UV lithography and Ti/Ni (50 nm/120 nm) was deposited by electron-beam evaporator to serve as a metal etch-mask. After metal lift-off, arrays of circular Ti/Ni metallization remained with diameters (D) ranging from 10 μm to 250 nm and pitches from 20 μm to 500 nm. For inductively coupled plasma (ICP) etching, the wafers were diced into 20 mm \times 20 mm square pieces and mounted on a Si carrier wafer coated with 50 nm atomic layer deposited Al_2O_3 . The samples were etched in an Oxford PlasmaLab 100 ICP system with an Oxford remote ICP380 source. After the ICP etching, the samples were put in $\text{HF}:\text{HNO}_3:\text{H}_2\text{O}$ (1:1:10) solution for 2 min to remove the etch mask and clean both etch debris and redeposited materials.

The samples were then observed in a field-emission scanning electron microscope (FESEM, Hitachi S4700). An integrated HORIBA Jobin Yvon's LabRAM 800HR bench-top system was used for PL (Kimmon He-Cd, 325 nm) and Raman spectroscopy (Laser Quantum DPSS, 532 nm) measurements with typical laser spot sizes of $\approx 50 \mu\text{m}$ and $\approx 1 \mu\text{m}$, respectively.

For post-ICP damage removal, 10% (mass fraction) KOH in ethylene glycol solution was used. For an isotropic wet etching of silicon, the samples were dipped in $\text{HF}:\text{HNO}_3:\text{CH}_3\text{COOH}$ (1:25:25) solution at room-temperature for 1 min.

III. RESULTS AND DISCUSSION

A. Effects of substrate temperature during ICP etch

Figures 1(a)–1(f) present FESEM images of etched pillars with 10 μm and 250 nm diameter starting circular patterns etched using $\text{Cl}_2/\text{N}_2/\text{Ar}$ (25/5/2 sccm) gas mixture at three different substrate temperatures (T): -120°C , 40°C , and 350°C . The other etch parameters such as ICP power (800 W), RF power (300 W), pressure (5 mT), and etching time (5 min) were kept constant. At lower etch temperature, significant tapering of the side wall angle was seen in smaller diameter structures. Figure 1(d) shows the cone shape pillars with base diameter of 680 nm and sloped sidewall angle of 75° . For smaller diameter pillars [Fig. 1(d)], significant lateral etching of the metal mask at -120°C can be seen and this is probably the cause for the formation of sharp tips. Similar phenomenon has been reported earlier.¹⁵ Also, it is interesting to note that the sidewall angle increases with increasing temperature. Sloped sidewalls at lower temperatures indicate a sputter-dominated regime with limited volatility of etch products;¹⁵ at lower cathode temperatures, the etch product (GaCl_3) might be solid given its melting point is 77.9°C at atmospheric pressure. As the temperature increases, the rate of chemical etching increases, which enhances uniform lateral etching of the sidewalls, leading to vertical NP sidewalls at 350°C as shown in Fig. 1(f).

B. Optical properties of etched pillars

Optical properties of those NPs have been measured using PL [Fig. 2(a)] and Raman spectroscopy [Fig. 2(b)] in order to understand the strain relaxation of GaN-on-Si structures as

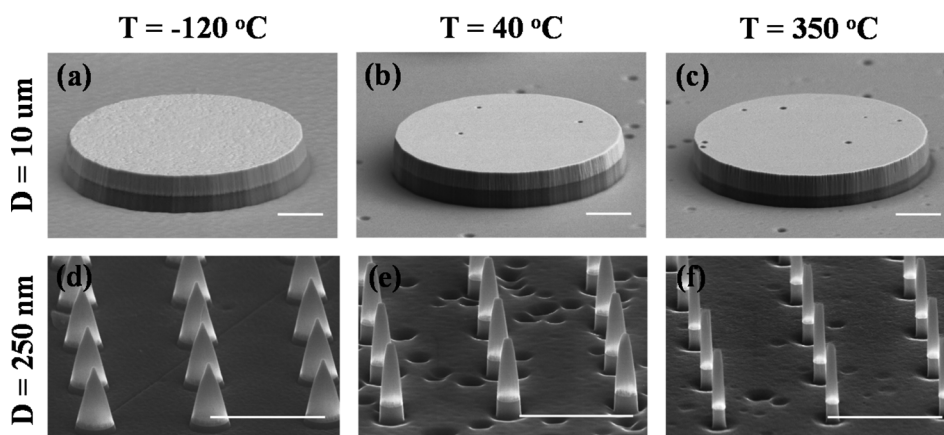


Fig. 1. FESEM images of GaN pillars etched using the indicated diameter (D) of metal mask and substrate temperatures (T) in $\text{Cl}_2/\text{N}_2/\text{Ar}$ (25/5/2 sccm). The scale bars indicate 2 μm .

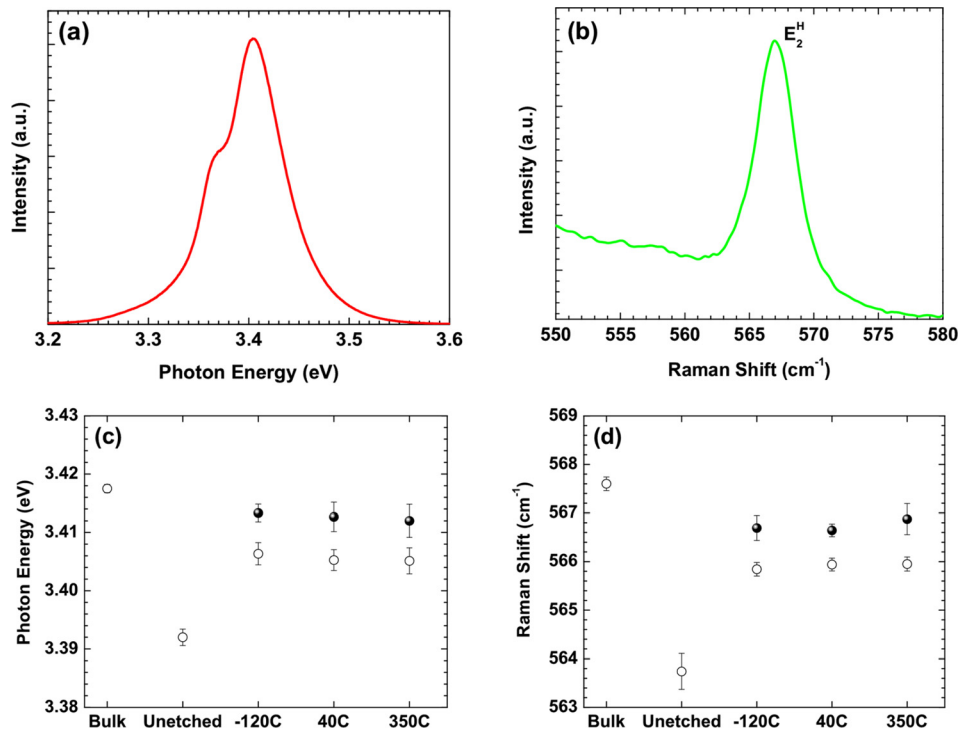


Fig. 2. (Color online) Representative room temperature (a) near band edge PL and (b) Raman E_2^H spectra of the pillars fabricated with metal mask of $D = 0.25 \mu\text{m}$ at 350°C . The peak positions of the pillars made from various mask sizes in Fig. 1 are also shown in (c) and (d). Open circles correspond to the pillars fabricated with metal mask of $D = 10 \mu\text{m}$ whereas the solid circles represent the same for $D = 250 \text{nm}$. The data for the bulk and unetched GaN samples (open circles) are also shown for comparison.

compared to the unetched films. Figure 2(c) represents the near band-edge (NBE) peak positions of the PL measured on the structures shown in Fig. 1. For comparison, we also included the NBE position from a free-standing, stress-free 3 mm thick GaN sample grown by halide vapor phase epitaxy method. As grown GaN films experience significant in-plane tensile stress due to the large mismatch in the thermal expansion coefficients between GaN and Si, which results in a red-shift of the NBE peak position in the PL as compared to the strain-free material.¹⁶ The clear blue shift of the NBE peaks for all the etched samples in Fig. 2(c) from the thin film value implies that the pillars are strain-relaxed compared to the GaN thin film. Similar compressive stress relaxation was observed in GaN NPs fabricated on sapphire substrate.^{17,18} The level of strain relaxation is greater in structures etched from 250 nm features, as compared to $10 \mu\text{m}$ features. Figure 2(d) summarizes the E_2^H peak position of Raman scattering for different structures shown in Fig. 1. The same trend is also evident in Raman scattering measurement, i.e., blue-shift of the etched structures indicates strain-relaxation due to ICP etching. In addition, the E_2^H mode for NPs etched at 350°C in Fig. 1(f) appears to be shifted toward higher wavenumber as compared to others. Thus, these NPs fabricated at higher temperature appear to be most strain-relaxed, which is not surprising considering their smallest overall diameter.

C. Gas chemistry dependent etching behavior

The morphologies of the NPs fabricated at room temperature using different gas chemistries are shown in

Fig. 3. By measuring the height of the NPs etched at different etch conditions, it is clear that the etch rate is much lower for the $\text{Cl}_2/\text{H}_2/\text{Ar}$ (25/5/2 sccm) chemistry than for $\text{Cl}_2/\text{He}/\text{Ar}$ (25/5/2 sccm) and $\text{Cl}_2/\text{N}_2/\text{Ar}$ (25/5/2 sccm). Similar suppression of the GaN etch rate with addition of H_2 has been observed for Cl_2/Ar plasma and was attributed to the consumption of reactive Cl radical by H, forming HCl.¹⁹ Figure 3(c) shows the room temperature NBE PL spectra from these NPs. There is no significant shift in the peak position. However, NPs fabricated using the $\text{Cl}_2/\text{H}_2/\text{Ar}$ (25/5/2 sccm) chemistry exhibit the most intense PL peak. Although the surface areas and volumes are different for all three different etch structures, simple calculations indicate that these differences are not sufficient to account for the observed differences in the PL intensities of the three samples. The difference in PL intensities for the three different etch chemistries was consistent across all three samples. As decrease in the PL intensity can be associated with increase in surface nonradiative recombination of photocarriers, the highest NBE PL intensity observed for the H_2 chemistry could be attributed to the lower surface defect density produced by the etch. However, the pillar geometry can also affect the light-coupling efficiency, which can account for the observed PL intensity enhancement. Comparing atomic mass of hydrogen (1.007 amu), helium (4.002 amu), and nitrogen (14.006 amu), it appears that the smaller mass of hydrogen atom might lead to lower damage of the etched surface, when other gases and processing parameters are same in the etch process. Temperature-dependent etching behavior for different gas chemistries are currently under investigation.

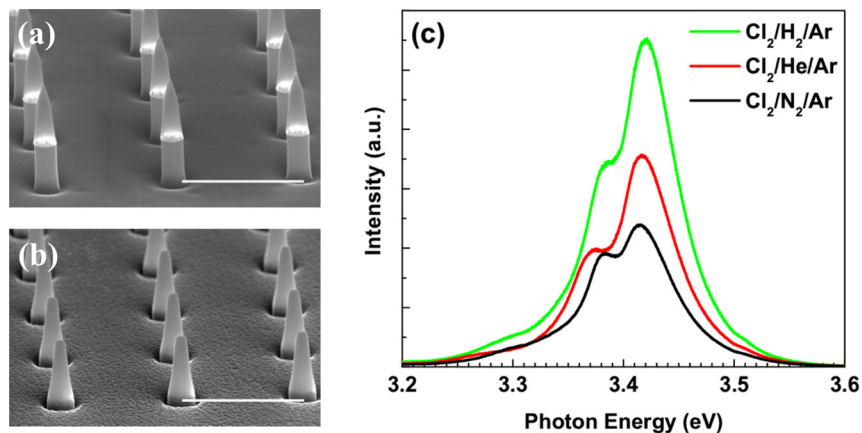


FIG. 3. (Color online) FESEM images of GaN NPs etched at different plasma chemistry: (a) $\text{Cl}_2/\text{He}/\text{Ar}$ (25/5/2 sccm) and (b) $\text{Cl}_2/\text{H}_2/\text{Ar}$ (25/5/2 sccm) at 40°C . The starting mask pattern was 250 nm diameter circles. For comparison, see Fig. 1(f) for $\text{Cl}_2/\text{N}_2/\text{Ar}$ (25/5/2 sccm) etch. The scale bars indicate $2\ \mu\text{m}$. The room temperature PL spectra are shown in (c).

D. Wet chemical etch of GaN pillars

Figures 4(a) and 4(b) show the morphology of the side-wall surface of GaN pillars after ICP etching and after subsequent wet chemical etching using 10 wt. % KOH in ethylene glycol for 10 min at 40°C . The KOH wet etching produced microfacets on the side walls but not on the top surface. The polarity-selective nature of KOH etching process is well-known, where N-polar planes are etched while Ga-polar planes remain unaffected due to the different states of the surface bonding.²⁰ Stocker *et al.* reported the evolution of $\{10\bar{1}0\}$ plane by etching cleaved GaN in 10 wt. % KOH dissolved in ethylene glycol at 165°C .²¹ The reported etch-rate for the m-plane in (10 50)% KOH in ethylene glycol at 90°C was 1.5 nm/min, whereas etch rate for c-plane was insignificant.²¹ Thus, it is most-likely that the microfacets observed on the side walls here are the $\{10\bar{1}0\}$ planes. To study the effectiveness of KOH based etchant for plasma etch-damage removal, the temperature was kept relatively low (i.e., 40°C) to ensure very slow etch rate. Under these conditions, the KOH wet etching produced surface texturing on the side walls of the GaN NPs [Fig. 4(b)]. Significant enhancement in the room temperature PL intensity was

observed after the KOH etching as compared to the ICP etched NPs [Fig. 4(c)]. This PL intensity enhancement could result from the removal of the surface plasma-induced defects (acting as nonradiative recombination centers) or from enhanced light extraction due to the texturing of the side-walls, or both.

Smaller diameter (500 nm and 250 nm) NPs were also etched at higher temperature (80°C) with KOH in ethylene glycol for different duration (Fig. 5). For this study, we used $1.5\ \mu\text{m}$ thick GaN epilayer, etched down with $\approx 0.5\ \mu\text{m}$ of GaN remaining on the surface. This permitted longer etching duration in the KOH solution that would not have been possible if Si was exposed at the base of these pillars. Preferential etching of Si would have resulted in removal of the pillars from the surface. Microfacets are evident after 20 min of etching. Reduction of the tapering with uniform diameters along the height of the NPs is observed after 120 min of etching. Reduction of the tapering can be explained by the removal of faster-etching planes, leaving slower-etching $\{10\bar{1}0\}$ m-planes along the height of the pillar. In recent years, there has been a significant push for the development of active devices along the nonpolar planes of GaN. The absence of detrimental polarization induced

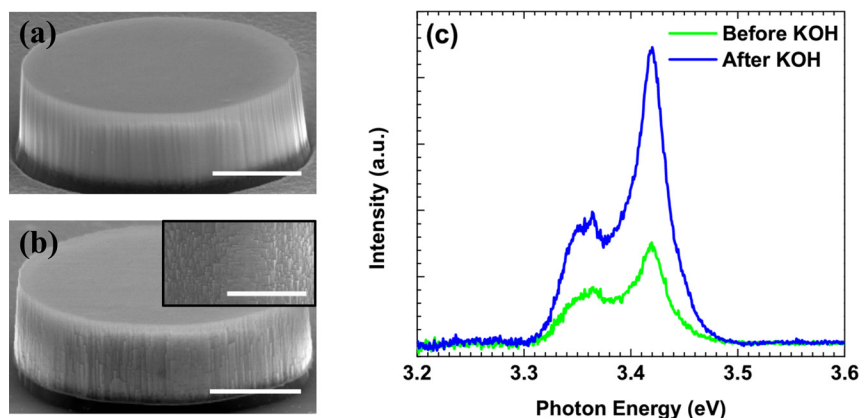


FIG. 4. (Color online) FESEM images of GaN NPs etched after (a) ICP etching at $T = 40^\circ\text{C}$, and (b) followed by wet etch in a solution of (10%) KOH in ethylene glycol. Inset image shows the magnified image of the side wall with surface texturing. The scale bars indicate $1\ \mu\text{m}$. (c) Room temperature PL spectra show the enhancement of the intensity after KOH treatment.

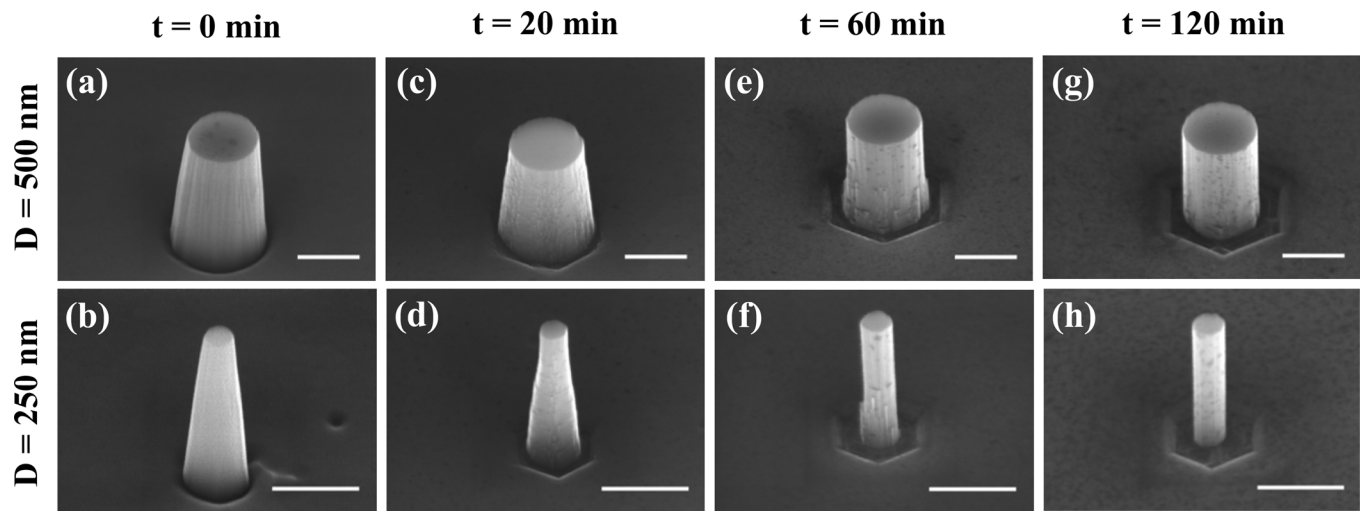


FIG. 5. FESEM images of KOH treated GaN NPs showing the evolution of different morphology as a function of different etching time (t). The wet chemical etch is carried out at 80°C using 10% KOH in ethylene glycol. NPs are fabricated using metal masks with 500 nm and 250 nm diameters. The scale bars indicate 500 nm.

charges and associated electric field in the nonpolar devices is the key in realizing high-performance light-emitting devices. Thus, the NPs with vertical sidewalls can be used as templates for engineering device heterostructures with active nonpolar interfaces.

E. Micro- and nanodisk structures

There have been a number of reports regarding the fabrication of nitride based microdisks using various selective chemical etching methods.^{22–24} However, those reported structures are very large with diameters ranging from $5\ \mu\text{m}$ to $200\ \mu\text{m}$ with rough side walls. By using selective wet chemical etch, we realized free-standing arrays of GaN micro- and nanodisks on Si (Fig. 6). The wet chemical etching was done using a solution of HF, HNO_3 , and CH_3COOH (HNA) at room temperature to selectively etch the Si at the base of the GaN pillars producing an undercut. GaN micro-disk structures show top diameter of $2\ \mu\text{m}$ with Si base pillar

with $1\ \mu\text{m}$ diameter [Fig. 6(a)]. The GaN nanodisks have top diameter of 500 nm with fine Si nanopillar with 50 nm diameter [Fig. 6(b)]. The etching rate of Si is very sensitive to the etchant solution temperature and etching time. At 25°C , the etching rate of Si is found to be $(400\text{--}500)$ nm/min while the etching rate of GaN is negligible. The GaN micro- and nanodisks with small diameter, smooth sidewalls, and good uniformity over a large area can thus be fabricated on the same substrate. Raman spectroscopy data of these nanodisks are compared with that of as-grown film in Fig. 6(c). The E_2^{H} peak positions for GaN thin film and nanodisk structures are found to be at 564.2 and $566.3\ \text{cm}^{-1}$, respectively. This indicates that the nanodisk structures are more strain-relaxed as compared to the as-grown GaN-on-Si film. Furthermore, a large increase in the Raman scattering intensity is observed from the nanodisk structures. This enhancement might be due to more efficient coupling and multiple scattering of light enabled by the large dielectric contrast of the air gap beneath the GaN surface as reported earlier.²³ These small

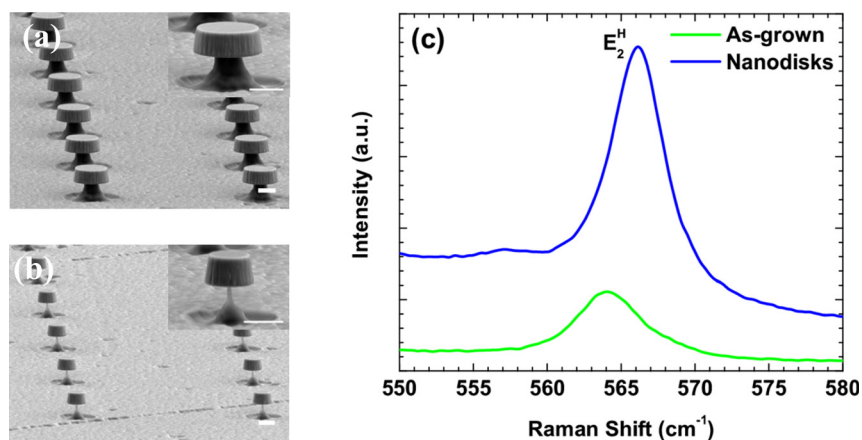


FIG. 6. (Color online) FESEM images of GaN (a) micro- and (b) nanodisk arrays fabricated using ICP etch and subsequent selective Si etching by HNA solution (The scale bars are $1\ \mu\text{m}$; the inset scale bars are 500 nm.) Inset in (a) shows a single microdisk with diameter of $2\ \mu\text{m}$ with base silicon undercut diameter of $1\ \mu\text{m}$; inset in (b) shows a single nanodisk with diameter of 500 nm with base Si undercut diameter of 50 nm. (c) Room temperature Raman scattering spectra from the nanodisk structures along with the as grown film.

diameter nanodisk structures might be useful for GaN based resonant cavity devices as well as low-power nanolaser.

IV. SUMMARY AND CONCLUSION

We have studied the surface morphology and optical properties of GaN micro and nanopillars fabricated using a combination of ICP and wet chemical etching of GaN epilayers grown on Si. Stress reduction has been achieved due to the reduction of constraining interfaces in these nanostructures. Etch damage resulting from different ICP processes was compared using PL, and post-ICP wet chemical etching treatment was studied as a means for its removal. This paper establishes a top-down methodology that effectively combines lithography, plasma-etch, and chemical-etch for fabrication of high-quality GaN micro- and nanostructures on Si substrate that can be utilized for high-quality vertical nano LEDs, UV photodetectors, and other photonic and electronic device.

ACKNOWLEDGMENTS

The nanostructures were fabricated at the Nanofab clean room of the NIST Center for Nanoscale Science and Technology. The University of Maryland portion of the work was partially supported by the Defense Threat Reduction Agency, Basic Research Award # HDTRA1-10-1-0107. One of the authors (R.D.) acknowledges the financial support through NIST-ARRA Senior Fellowship at the University of Maryland, College Park. Certain commercial equipment instruments or materials are identified in this paper to foster understanding. Such identification does not imply recommendation or endorsement by the National Institute of Standards and Technology nor does it imply that the materials or equipment identified are necessarily the best available for the purpose.

- ¹K. Chung, C. H. Lee, and G. C. Yi, *Science* **330**, 655 (2010).
- ²H. Matsubara, S. Yoshimoto, H. Saito, Y. Jianglin, Y. Tanaka, and S. Noda, *Science* **319**, 445 (2008).
- ³G. Fasol, *Science* **272**, 1751 (1996).
- ⁴H. Morkoç and S. N. Mohammad, *Science* **267**, 51 (1995).
- ⁵F. Qian, Y. Li, S. Gradecak, H. G. Park, Y. Dong, Y. Ding, Z. L. Wang, and C. M. Lieber, *Nature Mater.* **7**, 701 (2008).
- ⁶R. Yan, D. Gargas, and P. Yang, *Nature Photon.* **3**, 569 (2009).
- ⁷J. C. Johnson, H. J. Choi, K. P. Knutsen, R. D. Schaller, P. Yang, and R. J. Saykally, *Nature Mater.* **1**, 106 (2002).
- ⁸F. Qian, S. Gradečak, Y. Li, C. Y. Wen, and C. M. Lieber, *Nano Lett.* **5**, 2287 (2005).
- ⁹G. S. Aluri, A. Motayed, A. V. Davydov, V. P. Oleshko, K. A. Bertness, N. A. Sanford, and M. V. Rao, *Nanotechnology* **22**, 295503 (2011).
- ¹⁰S. Naureen, R. Sanatinia, N. Shahid, and S. Anand, *Nano Lett.* **11**, 4805 (2011).
- ¹¹S. Naureen, N. Shahid, A. Dev, and S. Anand, *Nanotechnology* **24**, 225301 (2013).
- ¹²S. Naureen, N. Shahid, R. Sanatinia, and S. Anand, *Adv. Funct. Mater.* **23**, 1620 (2013).
- ¹³R. Sanatinia, K. M. Awan, S. Naureen, N. Anttu, E. Ebraert, and S. Anand, *Opt. Mater. Express* **2**, 1671 (2012).
- ¹⁴R. Sanatinia, M. Swillo, and S. Anand, *Nano Lett.* **12**, 820 (2012).
- ¹⁵D. Paramanik *et al.*, *J. Vac. Sci. Technol. B* **30**, 052202 (2012).
- ¹⁶S. Krylyuk, D. Paramanik, M. King, A. Motayed, J. Y. Ha, J. E. Bonevich, A. Talin, and A. V. Davydov, *Appl. Phys. Lett.* **101**, 241119 (2012).
- ¹⁷Y. D. Wang, S. J. Chua, S. Tripathy, M. S. Sander, P. Chen, and C. G. Fonstad, *Appl. Phys. Lett.* **86**, 071917 (2005).
- ¹⁸F. Demangeot, J. Gleize, J. Frandon, M. A. Renucci, M. Kuball, D. Peyrade, L. Manin Ferlazzo, Y. Chen, and N. Grandjean, *J. Appl. Phys.* **91**, 6520 (2002).
- ¹⁹R. J. Shul *et al.*, *J. Vac. Sci. Technol. A* **16**, 1621 (1998).
- ²⁰D. Zhuang and J. H. Edgar, *Mater. Sci. Eng. R* **48**, 1 (2005).
- ²¹D. A. Stocker, E. F. Schubert, and J. M. Redwing, *Appl. Phys. Lett.* **73**, 2654 (1998).
- ²²A. C. Tamboli, E. D. Haberer, R. Sharma, K. H. Lee, S. Nakamura, and E. L. Hu, *Nature Photon.* **1**, 61 (2007).
- ²³H. W. Choi, K. N. Hui, P. T. Lai, P. Chen, X. H. Zhang, S. Tripathy, J. H. Teng, and S. J. Chua, *Appl. Phys. Lett.* **89**, 211101 (2006).
- ²⁴S. Vicknesh, S. Tripathy, V. K. X. Lin, L. S. Wang, and S. J. Chua, *Appl. Phys. Lett.* **90**, 071906 (2007).